RSC Advances

PAPER

View Article Online
View Journal | View Issue

Cite this: *RSC Adv.*, 2022, **12**, 9995

An efficient removal mechanism for different hydrophilic antibiotics from aquatic environments by Cu–Al–Fe–Cr quasicrystals†

Lei Zhang, [a] Tian Ai,*[a] Xiaoxi Tian[a] and Shujuan Dai[b]

The work studied the adsorption properties and mechanism of Cu–Al–Fe–Cr quasicrystals (QCs) for the adsorption of ibuprofen (IBU), tedizolid phosphate (TZD), and sulbactam sodium (SAM) for the first time. The experimental results showed that quasicrystals were good adsorbents with great potential. The structure, surface morphology, and elemental composition of QCs were investigated by XPS, XRD, SEM, EDX, particle size, DSC-TG, and FTIR. The adsorption pH, kinetics, thermodynamics, and isotherms of IBU, TZD, and SAM in QCs were systematically studied. QCs had good adsorption performance for antibiotics, and the adsorption capacities of IBU, TZD, and SAM were 46.964, 49.206, and 35.292 mg g^{-1} at the concentration of 25 mg L^{-1}, respectively. The surface charge and hydrophobicity of QCs were affected by changing pH, thereby affecting the adsorption performance of QCs. The main driving forces of adsorption included electrostatic force and hydrophobicity.

Received 4th November 2021
Accepted 22nd March 2022

DOI: 10.1039/d1ra08095d

rsc.li/rsc-advances

1. Introduction

Antibiotics are widely used in treating human and animal infections due to their unique antibacterial properties.[1] However, since most antibiotics are challenging for organisms to fully digest, they and their metabolites are discharged into the environment through excretions and urine.[2,3] Even though antibiotic concentrations are often detected at trace levels in the environment, they can still induce antibiotic resistance genes at a low concentration.[4] It can enhance the resistance of bacteria to drugs and have great hidden dangers for the evolution of the bacterial community structure.[5] Moreover, antibiotics may pose a huge threat to aquatic organisms such as fish when accumulated to high concentrations, because they have the characteristics of low biodegradability, high persistence, and easy bioaccumulation.[6,7] Therefore, antibiotics are considered as a new type of worldwide pollutants, and effective and sustainable water treatment technologies are urgently needed.[8]

Ibuprofen (IBU), one of the most widely sold antibiotics in the world, is a non-steroidal anti-inflammatory drug, mainly used as an anti-inflammatory, analgesic, and antipyretic.[9] However, according to American Time, long-term use of IBU can cause kidney failure. Sulbactam sodium (SAM) has a good effect on respiratory infections—inhibiting Staphylococcus, Escherichia coli, Haemophilus, and other bacteria.[9–11] However, it may cause allergic reactions to some people, rash, asthma, palpitations, and even anaphylactic shock.[12] Tedizolid phosphate (TZD) is a new anti-bacterial infection drug developed by Cubist Pharms, Inc. is an inhibitor of protein synthesis with a long half-life.[13] It plays an antibacterial role by inhibiting the synthesis of bacterial protein, mainly used in treating Gram-positive bacterial infection.[14] The hydrophilicity of these three antibiotics is quite different, so these three antibiotics were used to study the influence of hydrophilicity on the adsorption of materials to be studied in the work.

Removing antibiotics efficiently and environmentally is a challenge. Currently, mainly microbial-based treatment systems are insufficient to remove antibiotics with low degradability, high solubility, and complex molecular structure from wastewater.[15] Therefore, scientists have developed electrochemical oxidation, chemical reduction, nanofiltration membrane, electrocoagulation, and adsorption methods to separate antibiotics from wastewater.[16] Adsorption refers to the accumulation or attraction of adsorbate molecules on the solid surface when the adsorbate contacts the adsorbent surface. The adsorption method is widely used because of its simple operation, strong flexibility, low cost, strong reusability, and wide application range.[6,17] Finding a suitable adsorbent is vital for adsorption. Metal-based composites have a high adsorption efficiency, fast adsorption speed, high recovery, and strong reusability, which are the hotspots of recent research.[18,19] For example, Linjie Wang *et al.* prepared ZnO-porous carbon (ZnO-C) composites using MOF-74 (Zn) as a precursor. It has high adsorption performance for organic pollutants in wastewater

[a]*School of Chemical Engineering, University of Science and Technology Liaoning, Anshan 114051, PR China. E-mail: zl3303064@163.com; asatsky@163.com; astxx@163.com*

[b]*School of Mining Engineering, University of Science and Technology Liaoning, Anshan, PR China. E-mail: shujuandai@163.com*

† Electronic supplementary information (ESI) available. See DOI: 10.1039/d1ra08095d

and good stability and reusability after multiple cycles of operation.[18] Besides, metal-based composites are studied at a later stage, and the prepared Fe_3C-porous carbon (Fe_3C-C) has excellent adsorption and peroxymonosulfate (PMS) activation even in complex water environments. Besides good magnetic properties and reusability, bisphenol A (BPA) has excellent degradation performance even at high concentrations.[19]

At the end of 1984, a new structure-quasicrystal was first discovered by D. Schechtman *et al.* in the laboratory, which significantly affected natural science.[20] It is a special structure between crystal and amorphous, with the rotational symmetry of amorphous and the long period translation order of crystals.[21] The structure-quasicrystal also has a series of unusual physical and chemical properties such as low surface energy, low friction coefficient, high hardness, and high tensile strength.[22] Therefore, quasicrystals are widely used in surface-modification materials, thermal insulation materials, aerospace materials, and structural materials.[23] The study of J. T. Hoeft shows that the i-$Al_{70}Pd_{21}Mn_9$ quasicrystal has a good adsorption effect on benzene molecules.[24] Cu–Al–Fe–Cr quasicrystals (QCs) is a quasicrystal material with excellent oxidation resistance, high hardness, and low thermal conductivity.[25] However, they cannot be used as structural materials due to their brittleness at room temperatures.[25] QCs have a multi-layer structure and pore structure, and the number of pores decreases with increased layers.[26] QCs as solid-phase adsorption materials in the aqueous solution are rarely reported in previous literature. QCs were chosen as adsorbents of three different hydrophilic antibiotics in the work to investigate their adsorption capacity and mechanism, which opens up a new direction for the extended application of QCs.

2. Materials and methods

2.1. Materials

The antibiotics including TZD (with purity > 99.0%) was purchased from Shandong Xinhua Pharmaceutical Co., Ltd. (Shandong, China); IBU (with purity > 99.0%) from Guangzhou Jufeng Pharmaceutical Co., Ltd. (Guangzhou, China); SAM (with purity > 99.0%) from Zhejiang Shengtong Biotechnology Co., Ltd. (Jinhua, China). Table S1 (see ESI†) presents detailed physicochemical properties.

The IBU standard solution was prepared by dissolving IBU in methanol and then diluted in deionized water. TZD and SAM standard solutions were prepared by dissolving TZD and SAM directly in deionized water. QCs were prepared by tribology and Surface Engineering Research Center of School of Mechanical Engineering, University of Science and Technology Liaoning, with their average particle size between 400–600 mesh. Deionized water was used throughout the work, and other chemicals used were in analytical grade without requiring further purification.

2.2. Characterization of QCs

The surface morphologies and elemental composition of QCs were analyzed by scanning electron microscopy (SEM) (Zeiss modelΣIGMA HD/VP, Japan) with an accelerating voltage of 15 kV, combined with energy-dispersive X-ray spectroscopy (EDX). The main components of QCs were detected by an X-ray diffractometer (XRD) (Bruker Discover D8, Germany). The surface elements of QCs were analyzed by X-ray photoelectron spectroscopy (XPS) (Thermo escalab 250xi, America). The Fourier infrared spectrometer (FTIR) (JASCO model FT/IR-410, Japan) was used to study the change of functional groups of QCs before and after adsorption; with the wavenumber range of 400–4000 cm^{-1}, and a resolution of 4 cm^{-1}. Under N_2 atmosphere, the thermal characteristics of the QCs were examined using a thermogravimetric analyzer (PerkinElmer model Diamond 6300, America) at a heating rate of 10 °C min^{-1} from 35 to 1000 °C.

A laser particle size analyzer (Battersize model BT-9300S, China) was used to measure the particle size distribution of QCs. The point of zero charge (PZC) was measured with potentiometric mass titration using an automatic titrator (848 Titrino plus). pH values in the process were completed using precise pH test papers and a digital pH meter (Rex Electric Chemical model PHS-3C, China). The concentration changes of adsorbents before and after adsorption were completed by a UV spectrophotometer (model UV-1700SP C, Shanghai Meizan Instrument Co., Ltd., China). All drawings were completed by software Origin 2019.

2.3. Batch adsorption

Intermittent adsorption experiments were performed to study the adsorption of IBU, SAM, and TZD by QCs. In all experiments, 25 mg QCs were mixed with 50 mL adsorbates in a brown conical flask and were oscillated at a rate of 150 rpm in a thermostatic orbital shaker (Scigenics Biotech model Orbitek, India). After reaching adsorption equilibrium, the 0.45 μm regenerative fibrous membrane was used for filtration. The influence of different conditions on the adsorption effect was studied by the control variable method. 0.1 M HCl and 0.1 M NaOH solution were used to adjust the initial pH of the adsorbate solution to the range of 1–12. The adsorption effect of the adsorbate solution was tested 480 minutes to study adsorption kinetics. The pseudo-first-order model, pseudo-second-order model, and internal diffusion model were used to study the effect of time on adsorption. The adsorption isotherms were studied at an adsorbate concentration of 5–100 mg L^{-1} and the progressive one-fit analysis was performed by Langmuir, Freundlich, Tempkin and D–R models. Thermodynamic studies were also performed at 385, 390, 395, 400, 405, 410 and 415 K. All experiments were repeated twice to prevent large accidental errors.

2.4. Analysis of adsorbate

The concentration of adsorbate solution before and after adsorption was measured by a UV spectrophotometer (model UV-1700SP C, Shanghai Meizan Instrument Co., Ltd., China). The calibration curves of IBU, SAM, and TZD (R^2 = 1.0000, 0.9972, and 0.9964, respectively) were performed in the concentration of 0–100 mg L^{-1}, and the detection wavelengths

were set to 273, 230, and 300 nm, respectively. Based on the data obtained, their adsorption capacity was calculated according to the following formula:

$$q_e = \frac{(C_0 - C_1)V}{M} \quad (1)$$

$$q_t = \frac{(C_0 - C_t)V}{M} \quad (2)$$

where q_e (mg g^{-1}) is the adsorption amount adsorbed at equilibrium; q_t (mg g^{-1}) the adsorption amount adsorbed at time t; C_t (mg L^{-1}) the concentration of adsorbate at time t; C_0 (mg L^{-1}) and C_1 (mg L^{-1}) are the initial and equilibrium concentrations of adsorbate; M (g) is the mass of the adsorbent; V (L) the volume of the solution.

2.5. Recyclability tests of QCs

The reusability and stability of QCs were tested through five cyclic adsorption experiments in the work. The 50 mL, 25 mg L^{-1} adsorbate solution, and 25 mg quasicrystals were mixed in a brown conical flask, and then pH and temperature were optimized for adsorption. After a period of shaking in the shaker, a filter membrane was used to filter the 5 mL solution, and its concentration was measured in the ultraviolet spectrophotometer. The remaining solution was filtered and separated by filter papers. Then wash ultrasonically for 15 min by 10 mL methanol (IBU), and use 10 mL deionized water (SAM and TZD) as the regenerant. Filter again and dry at 110 °C to obtain the adsorbate for the next recycling. This cycle was repeated five times.

2.6. Data analysis

The pseudo-first-order model (3), pseudo-second-order model (4), and Intra-particle diffusion model (5) were used to fit and evaluate the kinetic data of QCs' adsorption. Detailed procedure calculating of adsorption results was explained in Text S1 (see ESI†).

Langmuir (6), Freundlich (7), Tempkin (8), and D–R (9) models were used to fit and analyze the isotherms data, thus determining the maximum adsorption capacity of QCs to adsorbates. The theory behind each model is given in Text S2 (see ESI†).

The thermodynamic parameters of the standard Gibbs free energy (ΔG°) (10), the enthalpy change (ΔH°) (11), and the entropy change (ΔS°) (12) were calculated to evaluate the thermodynamic behavior of QCs on adsorbates. Text S3 (see ESI†) shows the detailed calculation.

3. Results and discussion

3.1. Characterization of QCs

Fig. 1 shows the particle size distribution of QCs, and Table S2† shows the main data. The distribution of QCs is mainly concentrated in the range of 5–75 μm. The average particle size is 19.6 μm (Dx (50)); 10% of the particle size is less than 10.7 μm (Dx (10)); 10% of the particle size is greater than 35.6 μm (Dx (90)).

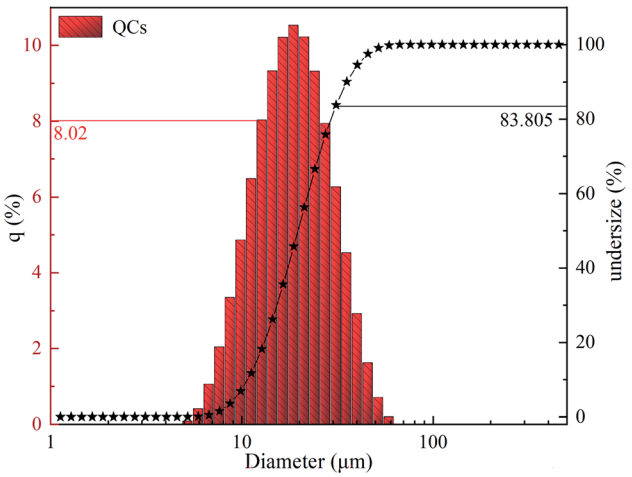

Fig. 1 Particle size distribution of QCs.

The surface elements of QCs were studied by XPS. Wide-scan XPS spectra (see Fig. S1(a)†) show that QCs contain Al, Cu, Fe, and Cr. The peak of Al is stronger, indicating higher Al content in QCs. It is consistent with the results detected by XRD. Narrow-scan XPS spectra (see Fig. S1(b)–(e)†) show that the intensity of the Al2p spectrum is the strongest. There are two peaks—one at 74.0 eV belongs to the quasicrystalline phase; the other at 75.5 eV belongs to alumina.[27] The peaks of Cu2p, Fe2p, and Cr2p are relatively weak, indicating that the oxides of Cu, Fe, and Cr on the QCs surface are not abundant. The reason is that the aluminum oxides on the surface boundary of QCs inhibit the further oxidation of Cu, Fe, and Cr. Narrow-scan XPS spectra indicate that the valence of Cu, Al, Fe, and Cr is not unique, showing that QCs may be composed of various substances.

The composition of QCs crystal is characterized by X-ray diffraction (XRD). Fig. 2(a) shows QCs are mainly composed of $Al_{65}Cu_{20}Fe_{10}Cr_5$ (PDF No. 42-1208), $Al_{82}Fe_{18}$ (PDF No. 45-1177), $AlFe_3$ (PDF No. 50-0955), and Cr (PDF No. 88-2323). SEM images and EDX images present many pores on the surface of $Al_{65}Cu_{20}Fe_{10}Cr_5$, which provides the necessary conditions for adsorption.[28] Therefore, $Al_{65}Cu_{20}Fe_{10}Cr_5$ is the substance mainly used for adsorption in the composition of QCs. After the repeated cyclic adsorption of IBU (see Fig. 2(b)), TZD (see Fig. 2(c)), and SAM (see Fig. 2(d)), we performed XRD again for adsorbed QCs. In Fig. 2, no significant change exists in the crystal lattice and phase of QCs before and after adsorption, so QCs are stable adsorbents.

DSC-TG mass-loss analysis is performed at 35–1000 °C to evaluate the stability of samples (see Fig. S2†). The mass of QCs decreases at 35–85 °C, and the endothermic peak at 85 °C is mainly attributed to the evaporation of free water in QCs. However, when the temperature is greater than 100 °C, the mass of QCs increases with the increased temperature. The exothermic peak at 615 °C is due to the interdiffusion of $Al_{82}Fe_{18}$, $AlFe_3$, Cr, and $Al_{65}Cu_{20}Fe_{10}Cr_5$ in QCs, which leads to

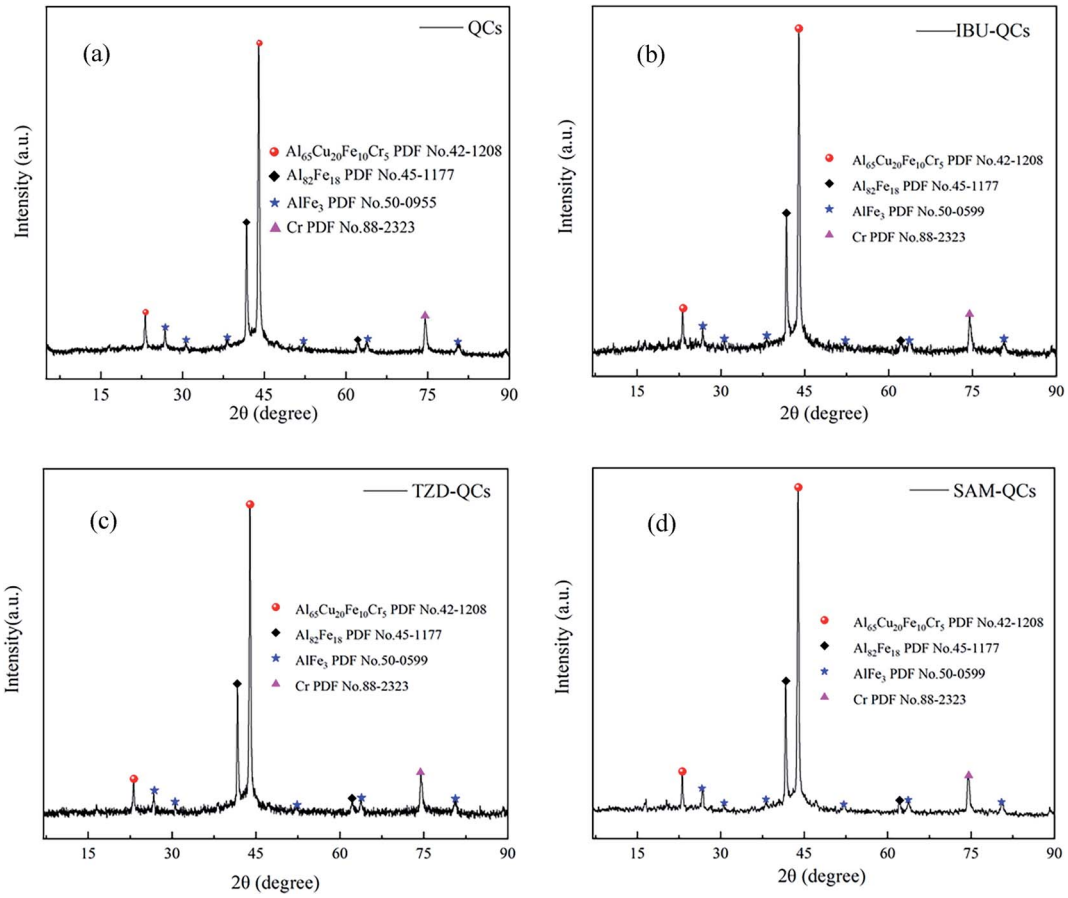

Fig. 2 (a) XRD pattern of QCs; (b) XRD pattern of QCs after IBU adsorption; (c) XRD pattern of QCs after TZD adsorption; (d) XRD pattern of QCs after SAM adsorption.

the unstable structure of quasicrystals and the formation of QCs with higher purity. Moreover, the increased mass is mainly caused by the adsorption of N_2 by QCs. The melting peaks appear between 790 and 810 °C, and the DSC values increased sharply between 810 and 845 °C, indicating that the melting point of QCs is near 845 °C.

The morphology of QCs is characterized by scanning electron microscopy (SEM). In Fig. 3, QCs are mainly composed of some regular spheres with different sizes and some irregular shapes. According to XRD and EDX, regular spheres may be $Al_{65}Cu_{20}Fe_{10}Cr_5$, while irregular shapes may be $Al_{82}Fe_{18}$, $AlFe_3$, and Cr. The regular spherical surface is arranged by some smooth regular polygons similar to fish scales.

It forms pores of different sizes at the sharp corners of the polygon, which makes a great contribution to adsorption. The interior takes the surface as a template and is self-organized with Cu into a layered structure,[29] which provides a great potential for multilayer adsorption. These irregular substances

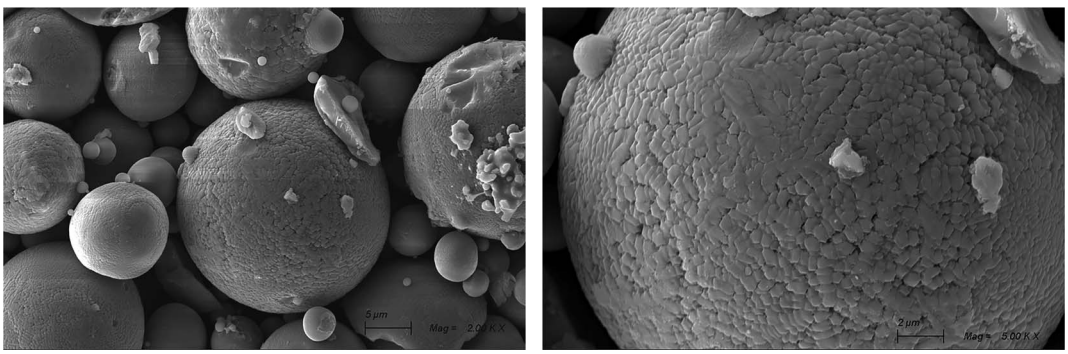

Fig. 3 SEM images (magnification 2000× and 5000×) of QCs.

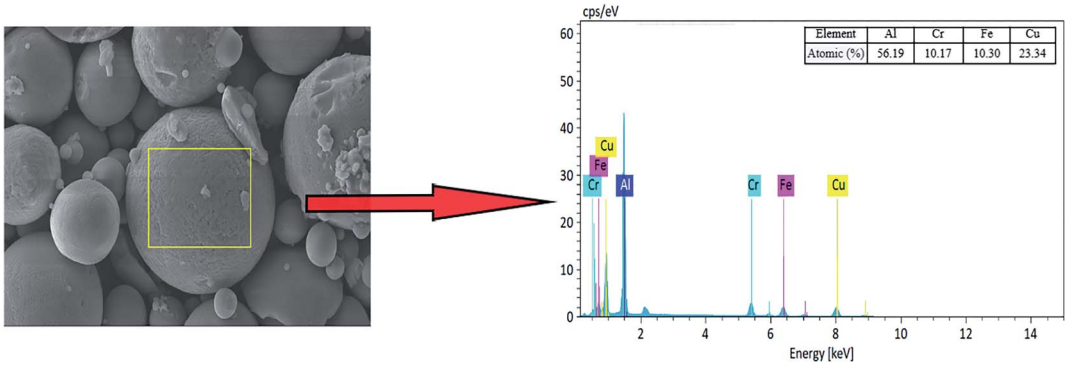

Fig. 4 Energy dispersive X-ray (EDX) spectrometry of QCs.

are attached to the sphere surface. Some places on the surface are concave, and the polygons on the surface become blurred. Thus, the irregular substances are embedded in the sphere instead of grafting due to extrusion. The concave position may be formed after the irregular substances fall off.

The EDX diagram (see Fig. 4) shows that the selected area is mainly the regular spherical surface and a small part of irregular substances. The main elements in the selected area are Al, Cr, Fe, and Cu, and the percentages of their atomic numbers are 56.19, 10.17, 10.30, and 23.34%, respectively. Therefore, combined with XRD, the regular spherical surface is mainly composed of $Al_{65}Cu_{20}Fe_{10}Cr_5$, which can determine adsorbent substances.

3.2. Effect of solution pH

Adsorption is a surface control process, so pH is an important parameter to study adsorption.[30] In this experiment, the pH of the solution was adjusted by adding HCl and NaOH. As shown in Fig. S3,† the adsorption capacity of QCs for IBU reached the optimal value of 46.96 mg g^{-1} at pH 4.5; at pH 2.0, the adsorption capacity of QCs for SAM and TZD reached the optimal values of 35.29 and 49.21 mg g^{-1}, respectively. When pH was greater than the optimum, the adsorption amount decreased rapidly and reached the minimum in alkaline conditions. Then it became stable.

When the pH of IBU, SAM, and TZD solution was less than their pK_a, the adsorbate in the solution was mainly cation; however, the zero charge point (see Table S2† for pHpzc) of QCs was 1.0. When pH > 1.0, the surface of QCs was a mainly negative charge. Therefore, when 1.0 < pH < pK_a, there was a strong electrostatic attraction between the adsorbate and the QCs, and the negative charge on the surface of QCs increased rapidly with increased pH.

Fig. S3† shows that the adsorption capacity increases with increased pH in the range of 1.0-pK_a and reaches the maximum when pH is about pK_a. When pH > pK_a, the adsorbate mainly exists as anions, and there is a strong electrostatic repulsion with the surface anions of QCs. Therefore, when pH > pK_a, the adsorption capacity of the QCs decreases sharply with increased pH.

Table S1† shows that IBU and TZD are insoluble and slightly soluble in water, respectively, and both contain hydrophobic-group phenyl (C_6H_5-). SAM is soluble in water, and the functional groups are hydrophilic. QCs are hydrophobic materials with a smooth surface and small friction coefficient. The adsorbate is driven by thermodynamic stability, and hydrophobic groups tend to accumulate on the quasicrystal surface to reduce surrounding water molecules.[31] Therefore, when the solution is alkaline, it still has weak adsorption due to the van der Waals force.

3.3. Adsorption kinetics

The equilibrium time and adsorption rate of the adsorption system can be evaluated by the relationship between the adsorption capacity and contact time and the kinetic model. Fig. 5(a) shows that the equilibrium adsorption time of TZD (450 min) and SAM (450 min) is much longer than that of IBU (150 min). The adsorption rates are extremely fast in the first 25 min, but the adsorption rate gradually slows down with time. The high initial solute concentration and more adsorption sites of the adsorbent result in a rapid initial adsorption rate. However, the solute concentration and the effective adsorption sites decrease with time, so the adsorption rate gradually decreases. The shorter time for IBU to reach the adsorption equilibrium is mainly due to the smaller molecular weight of IBU. Relatively, many effective adsorption sites can be adsorbed. Moreover, the negative charge on the QCs surface is more intensive and the electrostatic attraction is greater due to the greater pH of IBU solution, which makes IBU quickly transfer to the QCs surface.

The pseudo-first-order model (see Fig. 5(b)), the pseudo-second-order model (see Fig. 5(c)), and the intraparticle diffusion model (see Fig. 5(d)) are interpreted by piecewise fitting, respectively, to understand the adsorption kinetics characteristics. Table 1 shows the main parameters.

The pseudo-first-order model is mainly used to describe the rate at the initial stage of adsorption, but it is difficult to describe the entire adsorption process. Therefore, the pseudo-first-order model is not discussed in depth in the work.

The correlation coefficient of the pseudo-second-order model is slightly better than that of the pseudo-first-order model. However, the fitting effect of the pseudo-second-order model does not reach the ideal state, without explaining that

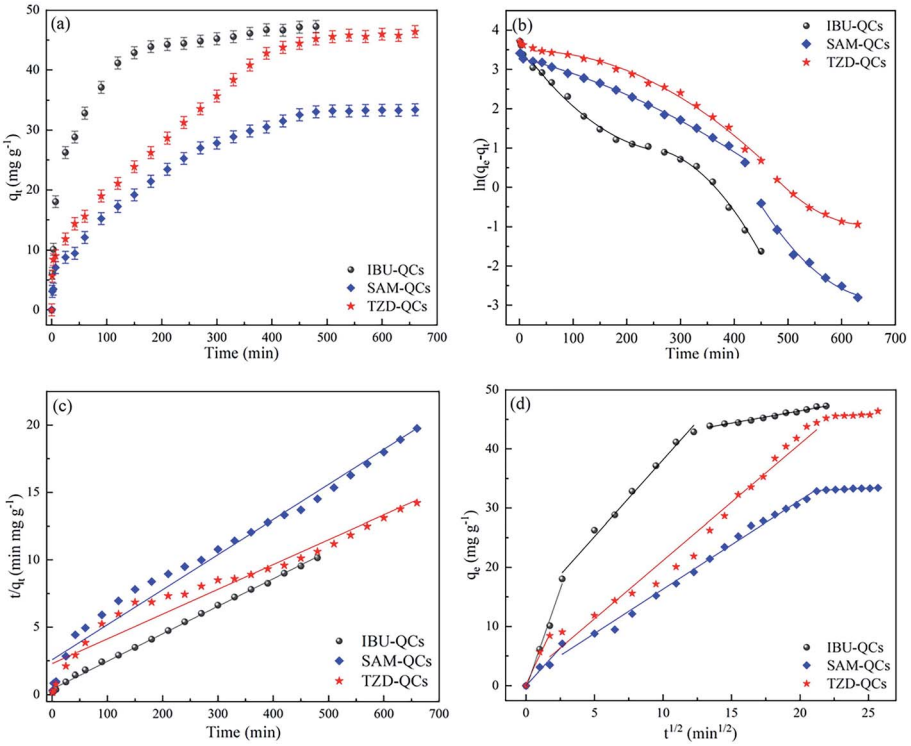

Fig. 5 (a) Effect of contact time on adsorption of antibiotics by QCs; (b) pseudo-first order model plot; (c) pseudo-second order model plot; (d) intra-particle diffusion kinetic plot.

Table 1 Parameters of pseudo-first-order, pseudo-second-order, and intraparticle diffusion kinetic model models for adsorbing IBU, TZD, and SAM on QCs (conditions: T = 25 °C; pH = 4.5 (IBU) and 2.0 (TZD and SAM); initial concentration of 25 mg L^{-1}.)

		Parameter value		
Kinetic model	Parameters	IBU-QCs	SAM-QCs	TZD-QCs
Pseudo-first-order	k_{f1} (min^{-1})	0.0217	0.0136	0.0171
	R_1^2	0.9907	0.9978	0.9946
	k_{f2} (min^{-1})	0.0375	0.0301	0.0179
	R_2^2	0.9980	0.9908	0.9978
Pseudo-second-order	k_s (g mg^{-1} min^{-1})	0.0009	0.0003	0.0002
	q_e (mg g^{-1})	49.43	38.41	54.31
	R^2	0.9991	0.9737	0.9412
Intraparticle diffusion	k_{ip1} (mg g^{-1} min$^{-1/2}$)	6.7065	2.7140	4.9083
	C_1	−0.4457	−0.0927	2.4322
	R_1^2	0.9891	0.9488	0.9886
	k_{ip2} (mg g^{-1} min$^{-1/2}$)	2.5924	1.4997	1.9709
	C_2	12.2449	1.3160	1.4406
	R_2^2	0.9910	0.9918	0.9918
	k_{ip3} (mg g^{-1} min$^{-1/2}$)	0.4324	0.1085	0.0912
	C_3	37.8134	30.6423	43.5001
	R_3^2	0.9874	0.9196	0.8632

the adsorption process should be controlled by chemical adsorption. Therefore, the adsorption process may be controlled by physical adsorption and chemical adsorption.

Since the pseudo-first-order and pseudo-second-order models cannot express the diffusion theory, the principle of adsorption kinetics is further analyzed by the internal diffusion model in Section 3.7.

3.4. Adsorption isotherm

Adsorption isotherm is a common method to describe the distribution of adsorbed molecules between the liquid phase and solid phase when the system reaches equilibrium.[31] The adsorption isotherm model can simulate the interaction between adsorbents and adsorbates. In Fig. S5,† the interaction

Table 2 Parameters of Langmuir, Freundlich, Tempkin, and D–R. (conditions: $T = 25$ °C; pH = 4.5 (IBU) and 2.0 (TZD and SAM); time = 480 min.)

Isotherm model	Parameter	Parameter value		
		IBU-QCs	SAM-QCs	TZD-QCs
Langmuir	q_m (mg g^{-1})	671.75	90.74	577.02
	k_L (L mg^{-1})	0.0024	0.0177	0.0028
	R^2	0.8376	0.9405	0.4077
Freundlich	k_f (mg g^{-1})	1.9086	4.0193	2.0063
	n	1.1573	1.6499	1.0790
	R^2	0.9995	0.9934	0.9916
Tempkin	K_T (L mg^{-1})	74.6707	16.7287	43.2626
	f	−2.3239	−1.2743	−2.0787
	R^2	0.9965	0.9911	0.9823
D–R	q_D (mg g^{-1})	112.17	36.06	82.47
	E (kJ mol^{-1})	0.0328	0.2093	0.0609
	R^2	0.9021	0.9811	0.9274

Table 3 Parameters of thermodynamic adsorbing IBU, TZD, and SAM on QCs (conditions: pH = 4.5 (IBU) and 2.0 (TZD and SAM); time = 480 min; initial concentration = 25 mg L^{-1}.)

Parameter	Temperature (K)	Parameter value		
		IBU-QCs	SAM-QCs	TZD-QCs
ΔG° (kJ mol^{-1})	285	−9.41	−3.61	−8.34
	290	−8.26	−3.55	−7.87
	295	−8.14	−3.39	−7.35
	300	−7.55	−3.28	−7.14
	305	−6.82	−3.20	−6.94
	310	−6.24	−3.04	−6.60
	315	−5.68	−2.98	−6.40
	320	−5.56	−2.81	−6.27
ΔH°(J mol^{-1})		−589.35	−145.73	−359.00
ΔS°(J mol^{-1} K^{-1})		−1.60	−0.33	−0.85
R^2		0.9913	0.9980	0.9806

mechanism between QCs and adsorbates is explained by fitting Langmuir (see Fig. S5(a)†), Freundlich (see Fig. S5(b)†), Temkin (see Fig. S5(c)†), and D–R (see Fig. S5(d)†) models. Table 2 shows the main parameters.

Fig. S4† shows that SAM and TZD have excellent adsorption effects when the solution concentration is less than 50 mg L^{-1}. However, the adsorption capacity has barely changed between 50–60 mg L^{-1}, and the adsorption capacity gradually increases when the solution concentration is more than 60 mg L^{-1}. However, the curve is flatter than that below 50 mg L^{-1}, which may be mainly related to multi-layer adsorption and vertical accumulation in the active center.[8,32] Compared with the Langmuir model (IBU: 0.8376, SAM: 0.9405 and TZD: 0.4077), the Freundlich model (IBU: 0.9995, SAM: 0.9933 and TZD: 0.9916) has better correlation coefficients (R^2), indicating that QCs follow the Freundlich adsorption isotherm model. Therefore, the adsorption of QCs belongs to multilayer adsorption.

In the first adsorption layer of the QCs' structure, the adsorption molecules enter a large gap, and the adsorption rate is the fastest. When it reaches saturation, the QCs surface aggregates more adsorbates and the relative pressure increased with the increased concentration, which reorientates the adsorbed substances in the internal pores.[32,33] The second adsorption layer is gradually formed when the concentration is 50–60 mg L^{-1}, providing more space for new adsorbate molecules. For IBU, its structure and molecular weight are relatively smaller and can enter smaller pores. Therefore, the second adsorption layer is not formed when the concentration is less than 100 mg L^{-1} (see Fig. S4†).

K_f is the affinity coefficient of Freundlich. Table 3 shows that their affinity order is as follows: SAM > TZD > IBU. However, QCs are hydrophobic. When adsorbate affinity is stronger, their hydrophilicity is stronger, resulting in weaker adsorption capacity, which corresponds to the experimental data. Parameter n known as the heterogeneity factor, is used to evaluate when the adsorption process is physical ($n > 1$), chemical ($n < 1$), or linear ($n = 1$).[34] Table 3 shows that adsorption is a physical process.

The Tempkin model describes the linear relationship between the decreased adsorption heat and adsorption capacity, which is suitable for heterogeneous surfaces.[35] In Table 3, Tempkin has an excellent fitting effect, indicating a strong electrostatic attraction between the adsorbate and the adsorbent.[36] It is consistent with the effect of pH.

K_T mainly reflects the adsorption heat. When $K_T > 1$, the adsorption process is mainly exothermic; when $K_T < 1$, it is mainly exothermic.[37] The K_T value is greater than 1 in the work, indicating that the adsorption process is exothermic. With the increased temperature, the hydrophobic effect weakens, resulting in decreased adsorption capacity.

E in the D–R model mainly reflects the adsorption energy. When the E value is in the range of 8–16 kJ mol^{-1}, the adsorption process is considered as an ion-exchange mechanism, which is chemical adsorption. When the E value is less than 8 kJ mol^{-1}, it is a physical adsorption process.[38] E values are less than 8 kJ mol^{-1} in the work, indicating that the adsorption process is mainly physical adsorption (consistent with Freundlich's judgment). However, the correlation coefficient (R^2) of D–R is relatively low, which cannot be used as a strong basis for judgment.

3.5. Adsorption thermodynamics

Adsorption energy is a powerful parameter to study the adsorption mechanism. In this experiment, the internal change of energy in the adsorption process was studied at 285–320 K. Table 3 shows the main parameters.

Fig. S6† shows the adsorption capacity presents a negative growth trend with the increased temperature. Besides, ΔH° is less than 0, indicating that the adsorption process is exothermic. With the increased temperature, the hydrophilicity of the adsorbate is enhanced, and the hydrophobicity of QCs is weakened, so the adsorption of QCs is reduced. ΔH° is less than 20 kJ mol^{-1} and the absolute ΔG° value decreases with the increased temperature, indicating that adsorption is a physical process. It is consistent with Freundlich's judgment.

The negative ΔG° value indicates that the whole adsorption process is spontaneous, which is attributed to the main role of

electrostatic attraction in the adsorption process. $\Delta S^{\circ} < 0$ indicates that the randomness of the solid–liquid interface decreases due to the orderly adsorption in the adsorption process. The adsorbate can form an orderly quasi-periodic coating in the unique position on the QCs surface, decorating the crystal lattice of quasicrystals.

3.6. Regeneration and reusability

The recycling of adsorbents can reduce the process cost and protect the environment. The reusability of adsorbents was explored through five repeated cycles in the work. The adsorbed QCs were dissolved in methanol (IBU-QCs) and deionized water (SAM-QCs and TZD-QCs) for regeneration and then dried at 110 °C for the next cycle. Fig. 6 shows that the adsorption capacity of QCs for the three adsorbates fluctuates in a small range ($\Delta q_e = \pm 2$ mg g^{-1}) in five cycles, indicating that QCs have excellent recyclable and stable adsorption. Therefore, QCs can be used for practical adsorption.

3.7. Adsorption mechanism

The intraparticle diffusion model is mainly used to predict the steps of speed control, depending on surface diffusion and pore diffusion.[39] In Fig. 5(d), the relationship between q_t and $t^{1/2}$ is nonlinear, indicating that the adsorption process may involve multiple processes.

Therefore, piecewise linear regression was used to describe different adsorption stages in the work. The first stage was the external surface transport stage with the steep curve, which is the fastest adsorption period. The second stage was gradual adsorption, and the curve tends to be smooth due to the diffusion of adsorbates through the pores of adsorbents. The third stage was adsorption equilibrium, and the curve was close to the level, because of the low adsorption of some micropores and the low concentration of adsorbates. Fig. 5(d) shows that the linear fitting does not pass through the origin, indicating that intraparticle diffusion is not the only mechanism for the adsorption of QCs.[40]

FTIR analysis was performed before and after adsorption to study the adsorption mechanism of QCs on antibiotics. After adsorption, multiple characteristic peaks of QCs can be found, indicating that QCs have a good adsorption effect on adsorbents. Compared with IBU, TZD and SAM before adsorption, the intensity of characteristic peaks of IBU-QCs, TZD-QCs, and SAM-QCs after adsorption decreases. The electrostatic attraction between QCs and adsorbents reduces the electronegativity difference between antibiotics and QCs, which weakens the absorption-peak intensity.[41]

Fig. 7 shows that some characteristic peaks in IBU, TZD, and SAM disappear, indicating that the adsorption of QCs significantly affects the functional groups of the adsorbent. The disappearance of the characteristic peak at the wavelength of 1640–1400 cm^{-1} due to the orderly adsorption in the adsorption process makes the benzene ring skeleton in the adsorbent form a more stable period on the QCs surface. The disappearance of characteristic peaks between 1300–1000 cm^{-1} is because of the stretching between the metal in QCs and the oxygen-containing functional groups of adsorbents,[42] with obvious characteristic peaks at about 519 cm^{-1}.

After adsorption, the characteristic peaks at 751 cm^{-1} in IBU migrates to 733 cm^{-1}; those at 3465 and 1630 cm^{-1} in TZD migrate to 3455 and 1641 cm^{-1}; those at 3460 and 1652 cm^{-1} in SAM migrate to 3477 and 1641 cm^{-1}, respectively. Besides, some peaks have a weak offset. The deviation of these peaks may be mainly due to the electron-induced effect between QCs and adsorbents.[43]

As a summary, the adsorption of QCs belongs to multi-layer adsorption, and the adsorption process is mainly shown in Fig. 8. The hydrophobic force is the main surface driving force so that antibiotics can be quickly adsorbed on the QC surface. Fig. 5(a) shows that the adsorption velocity within 10 min before

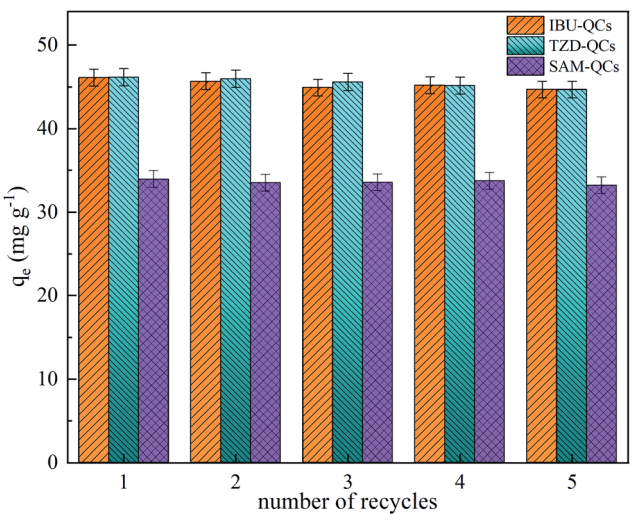

Fig. 6 Adsorption–capacity variation with recycles for regenerating QCs.

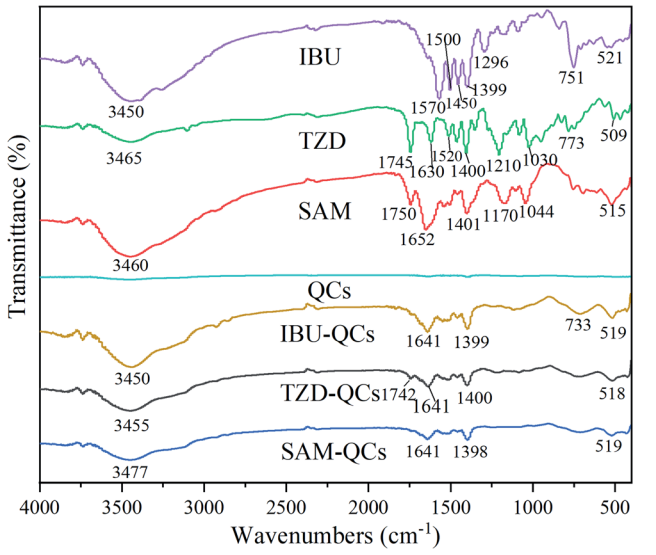

Fig. 7 FTIR spectra of QCs before and after adsorbing IBU, TZD, and SAM.

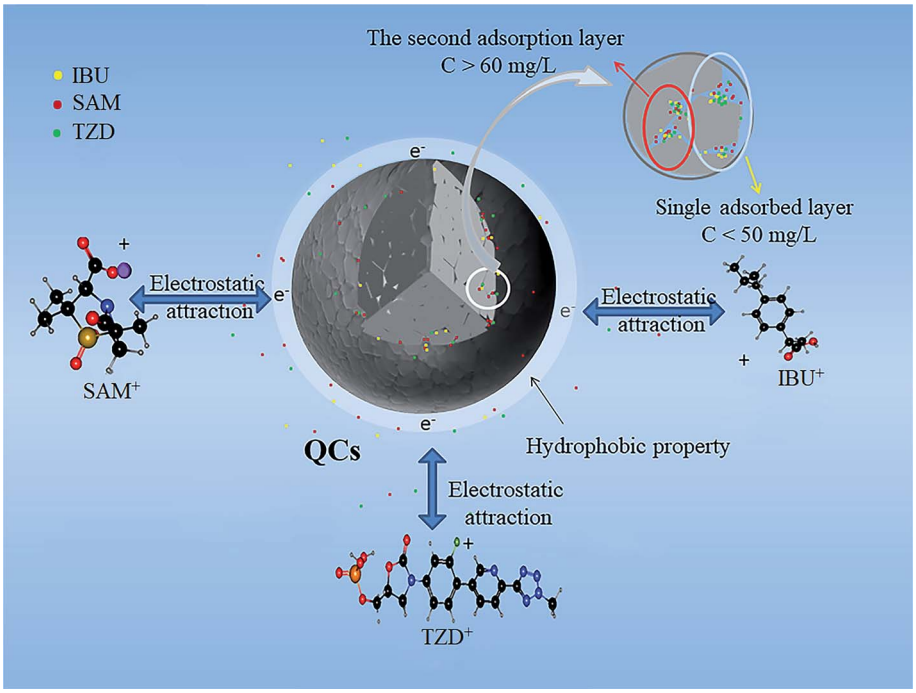

Fig. 8 Adsorption mechanism of QCs on IBU, TZD, and SAM.

adsorption is much higher than that after adsorption. As the antibiotic gradually accumulates in the surface pores and gradually reaches saturation, the adsorption capacity remains stable at the concentration of 50-60 mg L^{-1}. With the gradual accumulation of antibiotics on the surface, the pressure increases gradually. Antibiotics enter the second-layer pores of QCs when the concentration is greater than 60 mg L^{-1}, and the adsorption capacity increases. The adsorption process is mainly controlled by hydrophobic force, electrostatic attraction, and van der Waals force. The intensity of characteristic peaks before and after adsorption decreases, which can be proved by the shift of characteristic peaks.

4. Conclusions

QCs were first used to evaluate the adsorption capacities of IBU, SAM, and TZD in the work. The results showed that the adsorption capacities of QCs for IBU, SAM, and TZD were different. When the concentration was 25 mg L^{-1}, the maximum adsorption capacities of IBU, TZD, and SAM were 46.964, 35.292, and 49.206 mg g^{-1}, respectively. Through analyzing pH, adsorption isotherm, adsorption kinetics, and adsorption thermodynamics, the main driving force of adsorption was electrostatic attraction and hydrophobicity. Freundlich and Tempkin fit the adsorption isotherm of QCs, indicating that the adsorption of QCs was a spontaneous, physical, and multilayer adsorption process. The adsorption thermodynamic analysis showed that the adsorption process was exothermic. With the increased temperature, the hydrophobicity decreased, resulting in decreased adsorption capacity.

The particle-size analysis showed that the particle size of QCs was relatively concentrated, mainly distributed between 5–75 μm, and the average particle size was 19.6 μm. After five consecutive recycling experiments, the adsorption of QCs could reach more than 97% of the initial adsorption capacity. In short, QCs are efficient, stable, materials for a wide range of applications.

Conflicts of interest

The authors declare that they have no known competing financial interests or personal relationships that could have appeared to influence the work reported in this paper.

Acknowledgements

This work was financially supported by the National Natural Science Foundation of China (Grant Nos. 51874168 and 51574146), Innovation and Entrepreneurship Program of University of Science and Technology Liaoning (Grant No. X202010146234), and Xingliao Yingcai Science and Technology Innovation Leading Talent Project (Grant No. XLYC2002028).

References

1 Y. Gupta and A. S. Ghrera, *Arch. Microbiol.*, 2021, **203**, 3767–3784.
2 Y. Shen and X. Hao, *Sci. China: Life Sci.*, 2020, **63**, 1634–1650.
3 K. Qin, L. Wei, J. Li, B. Lai, F. Zhu, H. Yu, Qi. Zhao and K. Wang, *Chin. Chem. Lett.*, 2020, **31**, 2603–2613.
4 F. Reguyal, A. K. Sarmah and W. Gao, *J. Hazard. Mater.*, 2017, **321**, 868–878.

5 S. Harakeh, I. Khan, S. B. Almasaudi, E. I. Azhar, S. Al-Jaouni and A. Niedzweicki, *Curr. Drug Metab.*, 2017, **18**, 858–867.
6 W. Zheng, Z. Zhang, R. Liu and Z. Lei, *J. Environ. Sci.*, 2018, **65**, 8–17.
7 X. Liu, S. Lu and W. Guo, *Sci. Total Environ.*, 2018, **627**, 1196–1208.
8 K. Kha, A. K. Tareen, M. Aslam, R. U. R. Sagar, B. Zhang, W. Huang and A. Mahmood, *Nano-Micro Lett.*, 2020, **1**, 1–77.
9 F. D. Logu, S. L. Puma, L. Landini, T. Tuccinardi, G. Poli, D. Preti, G. D. Siena, R. Patacchini, M. G. Tsagareli and P. Geppetti, *Pharmacol. Res.*, 2019, **142**, 127–139.
10 L. K. Ruddaraju, S. V. N. Pammi, G. S. Guntuku, V. S. Padavala and V. R. M. Kolapalli, *Asian J. Pharm. Sci.*, 2020, **15**, 42–59.
11 B. Ding, B. Fang, J. Li, Q. Liu, C. Lv, X. Yu and X. Zhao, *Asian Pac. J. Trop. Med.*, 2020, **13**, 152–161.
12 D. Liu and X. Liang, *Chin. J. Integr. Med.*, 2017, **23**, 312–319.
13 R. Cao, J. Zhou and W. Chen, *Chin. J. Chem. Eng.*, 2020, **28**, 429–439.
14 Y. Lei, B. Jin, C. Ma, T. Zhang and T. Li, *J. Pharm. Biomed. Sci.*, 2017, **139**, 221–231.
15 X. Han, F. Yan, X. Nie, W. Xia, S. Chen, X. Zhang and L. Qian, *J. Integr. Agric.*, 2017, **16**, 640–647.
16 S. Jamaly, A. Giwa and S. W. Hasan, *J. Environ. Sci.*, 2015, **37**, 15–30.
17 A. Mustafa, B. G. Lougou, Y. Shuai, Z. Wang and H. Tan, *J. Energy Chem.*, 2020, **49**, 96–123.
18 L. Wang, P. Tang, J. Liu, A. Geng, C. Song, Q. Zhong, L. Xu and L. Gan, *J. Colloid Interface Sci.*, 2019, **554**, 260–268.
19 L. Gan, L. Wang, L. Xu, X. Fang, C. Pei, Y. Wu, H. Lu, S. Han, J. Cui, J. Shi and C. Mei, *J. Hazard. Mater.*, 2021, **413**, 125305–125320.
20 H. Xie, F. Liu, J. Zhang, C. Zhang and L. Ren, *Sci. China: Chem.*, 2011, **54**, 835–843.
21 Y. Xu, D. Xu, X. Shao, E. Han and G. P. Zone, *Acta Metall. Sin.*, 2013, **26**, 217–231.
22 L. Xing, Y. Xie, D. Minakata, H. Cao, J. Xiao, Y. Zhang and J. C. Crittenden, *J. Environ. Sci.*, 2014, **26**, 2095–2105.
23 W. Zhang, Z. Wei, L. Zhang, Y. Xing and Q. Zhang, *Rare Met.*, 2020, **39**, 352–367.
24 J. T. Hoeft, J. Ledieu, S. Haq, T. A. Lograsso, A. R. Ross and R. McGrath, *Philos. Mag.*, 2006, **86**, 869–874.
25 J. Kong, C. Zhou, S. Gong and H. Xu, *Surf. Coat. Technol.*, 2003, **165**, 281–285.
26 Y. Fu, N. Kang, H. Liao, Y. Gao and C. Coddet, *Intermetallics*, 2017, **86**, 51–58.
27 J. Bu, H.-K. Rhee, Y. Z. Shen and K. S. Shin, *J. Mater. Sci. Lett.*, 2001, **20**, 1165–1167.
28 Q. Song, Y. Fang, Z. Liu, L. Li, Y. Wang, J. Liang, Y. Huang, J. Lin, L. Hu, J. Zhang and C. Tang, *Chem. Eng. J.*, 2017, **325**, 71–79.
29 S. K. Pandey, K. Sunita, A. Bhatnagar and S. S. Mishra, *J. Phys. Chem. C*, 2017, **121**, 24936–24944.
30 J. Lin, X. Wang and Y. Zhan, *J. Environ. Sci.*, 2019, **76**, 167–187.
31 S. Yu, J. Liu, Y. Yin and M. Shen, *J. Environ. Sci.*, 2018, **63**, 198–217.
32 S. Álvarez-Torrellas, A. Rodríguez, G. Ovejero and J. García, *Chem. Eng. J.*, 2016, **283**, 936–947.
33 M. A. Bahri, L. Calvo, J. Lemus, M. A. Gilarranz, J. Palomar and J. J. Rodríguez, *Chem. Eng. J.*, 2012, **198**, 346–354.
34 A. C. Martins, O. Pezoti, A. L. Cazetta, K. C. Bedin, D. A. S. Yamazaki, G. F. G. Bandoch, T. Asefa, J. V. Visentainer and V. C. Almeida, *Chem. Eng. J.*, 2015, **260**, 291–299.
35 R. Aigbe and D. Kavaz, *Chin. J. Chem. Eng.*, 2021, **29**, 92–102.
36 Y. Sun, S. Luo, J. Xing, Z. Li and A. Meng, *J. Ocean Univ. China*, 2021, **20**, 349–360.
37 D. Kang, X. Yu, M. Ge, F. Xiao and H. Xu, *J. Environ. Sci.*, 2017, **54**, 1–12.
38 W. Wang, X. Zhang, Y. Zhang, X. Mi, R. Wang, H. Shi, C. Li, Z. Du and Y. Qiao, *Pedosphere*, 20201, **31**, 596–605.
39 T. B. CostaMeuris, G. C. SilvaMelissa and G. A. Vieira, *BBA-Bioenergetics.*, 2020, **38**, 339–355.
40 M. A. Chayid and M. J. Ahmed, *J. Environ. Chem. Eng.*, 2015, **3**, 1592–1601.
41 Y. Zhang, P. Wang, G. Sun, J. Yang and R. Gao, *J. Wuhan Univ. Technol.*, 2021, **36**, 446–455.
42 P. Hao, X. Ma, J. Xie, F. Lei, L. Li, W. Zhu, X. Cheng, G. Cui and B. Tang, *Sci. China: Chem.*, 2018, **61**, 797–805.
43 M. Jia, F. Wang and Y. Bian, *Bioresour. Technol.*, 2013, **136**, 87–93.